# Supporting Information

## Remarkable high-temperature ionic thermoelectric performance induced by graphene in gels thermocells

Cheng-Gong Han[1,‡,*], Yongbin Zhu[1,‡], Lijuan Yang[1,‡], Jiawei Chen[1], Shengjie Liu[1], Haoyu Wang[1], Yingming Ma[1], Dongxue Han[1], Li Niu[1,2,*]

1. Center for Advanced Analytical Science, Guangzhou Key Laboratory of Sensing Materials and Devices, Guangdong Engineering Technology Research Center for Photoelectric Sensing Materials and Devices, Key Laboratory of Optoelectronic Materials and Sensors in Guangdong Provincial Universities, School of Chemistry and Chemical Engineering, Guangzhou University, Guangzhou 510006, P. R. China.
2. School of Chemical Engineering and Technology, Sun Yan-sen University, Zhuhai 519000, P. R. China.

‡ These authors contributed equally to this work.

*Corresponding Email: hancg@gzhu.edu.cn (Cheng-Gong Han); lniu@gzhu.edu.cn (Li Niu)

**Note 1. The ionic thermopower of gels thermocell.**

For a redox couple contained gels thermocell, the electrochemical potential of electrons in the electrode will be affected by the redox reaction occurred at electrode/gels interface. For a redox reaction: $FeCN^{3-} + e \rightleftharpoons FeCN^{4-}$, the net change in electrochemical potential should be zero at both the hot electrode and the cold electrode when the redox reaction reach to an equilibrium. In this case,

$$\tilde{\mu}_{FeCN^{3-}}(T_H) + \tilde{\mu}_e(T_H) = \tilde{\mu}_{FeCN^{4-}}(T_H) \quad (1)$$

$$\tilde{\mu}_{FeCN^{3-}}(T_C) + \tilde{\mu}_e(T_C) = \tilde{\mu}_{FeCN^{4-}}(T_C) \quad (2)$$

As for electrochemical potential $\mu = \mu + qV$, it contains the chemical potential $\mu$ and electrostatic potential part $qV$, where $q$ is the charge and $V$ is the electrostatic potential across the gels.

$\mu_e = E_F - FV_e$ is the electrochemical potential of electrons (per mole) in the electrode, where $E_F$ is the Fermi level of electrode, $V_e$ is the electrostatic potential in the electrode, and $F$ is the Faraday constant.[S1] The Fermi level $E_F$ of electrode could be regarded as a constant due to the minor temperature difference. As a result, the difference of electrochemical potential of electrons in the electrode between the hot and cold sides is directly the voltage difference. Then we can obtain the following relation.

$$\begin{aligned}\Delta\tilde{\mu}_e &= \Delta\tilde{\mu}_{FeCN^{4-}} - \Delta\tilde{\mu}_{FeCN^{3-}} = \left(\Delta\mu_{FeCN^{4-}} - \Delta\mu_{FeCN^{3-}}\right) + \left(q_{FeCN^{4-}} - q_{FeCN^{3-}}\right)\Delta V \\ &= \left(\frac{\partial\mu_{FeCN^{4-}}}{\partial T} - \frac{\partial\mu_{FeCN^{3-}}}{\partial T}\right)\Delta T + (-nF)\Delta V \\ &= -\left(s_{FeCN^{4-}} - s_{FeCN^{3-}}\right)\Delta T + FS_{td}(K^+ - FeCN^{4-/3-})\Delta T\end{aligned} \quad (3)$$

where $\Delta$ means the quantity at the hot side minus the quantity at the cold side, and we used the relation $\frac{\partial\mu}{\partial T} = -s$ ($s$ means the entropy) and $S_{td}(K^+ - FeCN^{4-/3-}) = -\frac{\Delta V}{\Delta T}$ ($S_{td}$ means the ionic thermopower from thermodiffusion effect in gels).[S2]

Hence, the ionic thermopower

$$\begin{aligned}S_i &= \frac{\Delta\tilde{\mu}_e}{F\Delta T} = -\frac{\Delta V_e}{\Delta T} = -\frac{\Delta s}{F} + S_{td}(K^+ - FeCN^{4-/3-}) \\ &= S_{tg}(FeCN^{4-/3-}) + S_{td}(K^+ - FeCN^{4-/3-})\end{aligned} \quad (4)$$

**Note 2. Charicaterization of three different kinds of graphene.**

The GO (graphene oxide) was obtained by the oxidation of graphite. The rGO (reduced graphene oxide) was from the reduction of GO, displaying the decreased fuctional groups; as futher reducing GO, Gr (graphene) was fabricated and possessed the few fuctional groups.[S3] In Fig. S7,

the GO (graphene oxide) showed characteristic adsorption bands for the hydroxy -OH (3391 $cm^{-1}$), carboxyl C=O (1723 $cm^{-1}$), aromatic C=C (1621 $cm^{-1}$), epoxy C-O (1220 $cm^{-1}$) and alkoxy C-O (1043 $cm^{-1}$) groups.[S4] The oxygen contained fuctional groups indicated that the graphite was oxidated to GO. However, the peaks of carboxyl C=O (1723 $cm^{-1}$) and aromatic C=C (1621 $cm^{-1}$) disappeared and the broad and weakened peaks belonged to hydroxy -OH (3391 $cm^{-1}$), epoxy C-O (1220 $cm^{-1}$) and alkoxy C-O (1043 $cm^{-1}$) were observed for rGO and Gr. This indicated that the fuctional groups decreased as further reducing GO. The fuctionanl groups, such as -OH and C-O were still present in the employed rGO and Gr raw materials. For differentiating the rGO and Gr with the similar FTIR curves, the Raman spectra were conducted and shown in Fig. S8. Two distinct peaks of D at 1336 $cm^{-1}$ and G at 1570 $cm^{-1}$ were observed for GO, rGO, Gr, which the formmer was due to defects and disordered carbon and the latter was arised from the sp2-hybridized carbon atom.[S5,S6] The intensity ratio of D to G peaks ($I_D/I_G$) was usually employed to identify the degree of disorder of graphene.[S7] $I_D/I_G$ = 1.13, 1.09 and 0.26 were noticed for GO, rGO and Gr, respectively. The lowest $I_D/I_G$ for Gr indicated the lowest disorder due to the formation of mechanical exfoliation. The charicteristic G' peak was observed at 2700 $cm^{-1}$, which G' peak was used to evaluate the number of layers in a graphene.[S8] The high and wide G' peak indicated a residue of a few layers in the employed graphene. Consequently, three different kinds of graphene as GO, rGO, and Gr were distinguished by using FTIR and Raman spectra.

**Note 3. Ionic conductivity of gels.**

Electrochemical impedance spectroscopy (EIS) as an effective electrochemical technology, is employed to obtain the ionic conductivity of gels in this work. The resistance of gels thermocell is regard as the real part value based on the intercept of Nyquist plot in EIS. The ionic conductivity was calculated by the equation of $\sigma_i = \frac{d}{RS}$, where $d$, $S$ and $R$ are the thickness, section area and resistance, respectively. Herein, $d$ = 0.2 mm, $S$ = 100 $mm^2$. The platinum is severed as electrodes. EIS at different temperatures is measured in an isothermal system. In Fig S10, S11 and S12, the ionic conductivity at different temperatures was obtained.

Moreover, the relationship between ionic conductivity and diffusion coefficient could be given based on the Nernst-Einstein equation.[S9]

$$\sigma = \sigma_+ + \sigma_- = \frac{F^2}{RT}(v_+ z_+^2 D_+ + v_- z_-^2 D_-) \quad (5)$$

where $F$ is the Faraday constant, $R$ is the gas constant, $T$ is the thermodynamic temperature, $v_+$ and $v_-$ are the number of cations and anions per formula unit of electrolyte, $z_+$ and $z_-$ are the valences of

the ions, $D_+$ and $D_-$ are the diffusion coefficients of the ions. From the equation (5), the ionic conductivity should be related to the combination of the diffusion coefficient of cations and anions. The positive thermodiffusive thermopower $S_{td}$ (Fig. 3 (b)) suggests larger thermal mobility ( $\frac{D_+\hat{S}_+}{k_BT}$ ) of cations than that ( $\frac{D_-\hat{S}_-}{k_BT}$ ) of anions ($\hat{S}$ is the Eastman entropy of transfer).[S2]

**Note 4. Thermal conductivity of gels**.

The thermal conductivity of gels is obtained according to the following equation.

$$\kappa = D\rho C_p \tag{6}$$

where κ, $D$, $\rho$, and $C_p$ are the thermal conductivity, thermal diffusivity, average body density and specific heat capacity, respectively. We employed LFA (LFA457, NETZSCH) to measure the out-of-plane $D$ from 273 to 323 K. $\rho$ was determined according to the mass/volume method. $C_p$ of pure gelatin was used.[S2] Fig. S14 shows the thermal diffusivity and thermal conductivity of gels Gelatin-0.04/0.06 M $FeCN^{4-/3-}$-*x* wt.% Gr. No big changes were noticed for the thermal diffusive of gels as increasing temperatures. The thermal diffusive of gels with 6 wt.% Gr was higher than that of 0 wt.%. The thermal conductivity increased as the temperature increased. The thermal conductivity for 6 wt.% Gr was higher than that of 0 wt.% in the whole measured temperature range, showing the values from 0.10 to 0.21 W $m^{-1}$ $K^{-1}$.

**Note 5. Diffusion coefficient of redox couple ions.**

Cyclic Voltammetry (CV) can be used to investigate the redox reaction at the interface of gels/electrodes. For a redox couple contained gels, the characterization of ions participited in redox reaction could be reflected in the oxidation/reduction peaks. The diffusion coefficient of ions participited in redox reaction can be calcualted by the Randles-Sevcik equation: $i_p = 269000n^{3/2}ACD^{1/2}v^{1/2}$, where $i_p$, $n$, $A$, $C$, $\upsilon$ and $D$ were peak current, number of electrons, electrode area, ions concentration, scan rate and diffusion coefficient, respectively.[S10] By ploting the picture of $i_p$ vs. $\upsilon^{1/2}$, which $\upsilon$ sancs at the different rates, diffusion coefficient of ions is directly related to the slop of curve. In this work, the platinum was used as the electrodes in a $FeCN^{4-/3-}$ contained gelatin. CV curves are sanced from negtive to positive directions and the scan rates are 10, 30, 50, 70 mV $s^{-1}$, respectively. We employed the CV curve at the second cycle for obtaining the total diffuison coefficient of $FeCN^{4-/3-}$. The charicteristic anodic peaks were observed at 0.15-0.3 V. As the scan rates increased, the peaks shifted to a high voltage due to the polorization. Fig

S17, S18, S19 and S20 show the CV curves measured at different temperatures and the plot of $i_p$ vs. $v^{0.5}$. In this way, the diffusion coeffcient of $FeCN^{4-/3-}$ at different temperatuer was obtained.

**Note 6. Reactivation of gels thermocell after discharge stage**.

As shown in Fig. S24, all ions including $K^+$, $FeCN^{3-}$ and $FeCN^{4-}$ are distributed uniformly in gels at initial stage and no voltage is generated. In thermal charge stage, a combination of a redox reaction $FeCN^{3-} + e \rightleftharpoons FeCN^{4-}$ and thermodiffusion of $K^+$ and $FeCN^{4-/3-}$ result in a thermo-induced voltage under a temperature gradient. In the thermal discharge stage, an external load is connected to two electrodes of gels thermocell, forming the external output current. The current consists of two parts: Faradaic current from redox reaction and non-Faradaic current from thermodiffusion effect. During this thermally electric discharge process, an electrode polarization often occurs due to the non-Faradaic current, which negative and positive charges would accumulate near cold and hot electrode surface, respectively. As a result, such net surface charges increase, facilitating the physical adsorption of counterions, i.e. more $K^+$ adsorbed to the cold electrodes. Such adsorption would further lower the ions kinetics and redox reaction, suppressing the continuously high output performance. Reactivation could effectively decrease such delay because the ions can return back to their initial state at room temperature when removing temperature gradient.[S2]

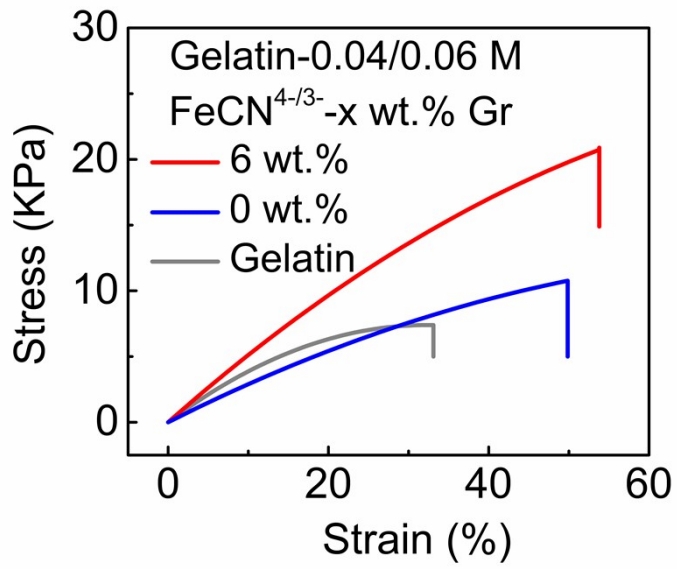


Fig. S1. Stress-strain curves of gels Gelatin-0.04/0.06 M $FeCN^{4-/3-}$-*x* wt.% Gr.

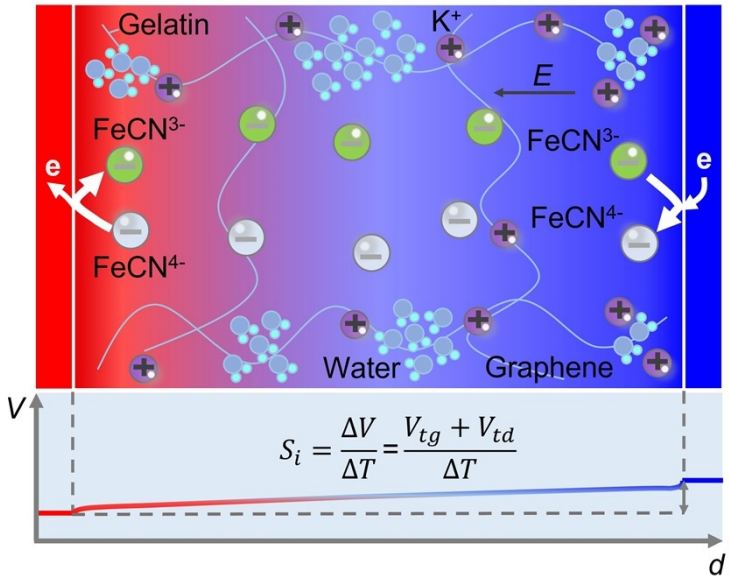


Fig. S2. Schematic of voltage generation of gels Gelatin-*m*/*n* $FeCN^{4-/3-}$ under temperature gradient ($T_H > T_C$).

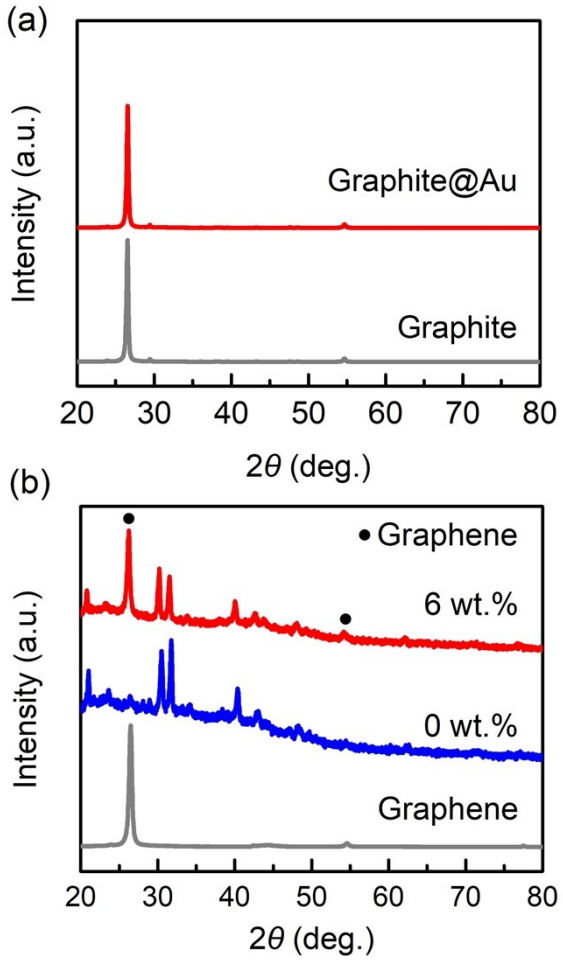


Fig. S3. X-ray diffraction patterns of (a) Graphite and Graphite@Au, and (b) Graphene (Gr), Gelatin-0.04/0.06 M $FeCN^{4-/3-}$-6 wt.% Gr ($x$ = 0, 6).

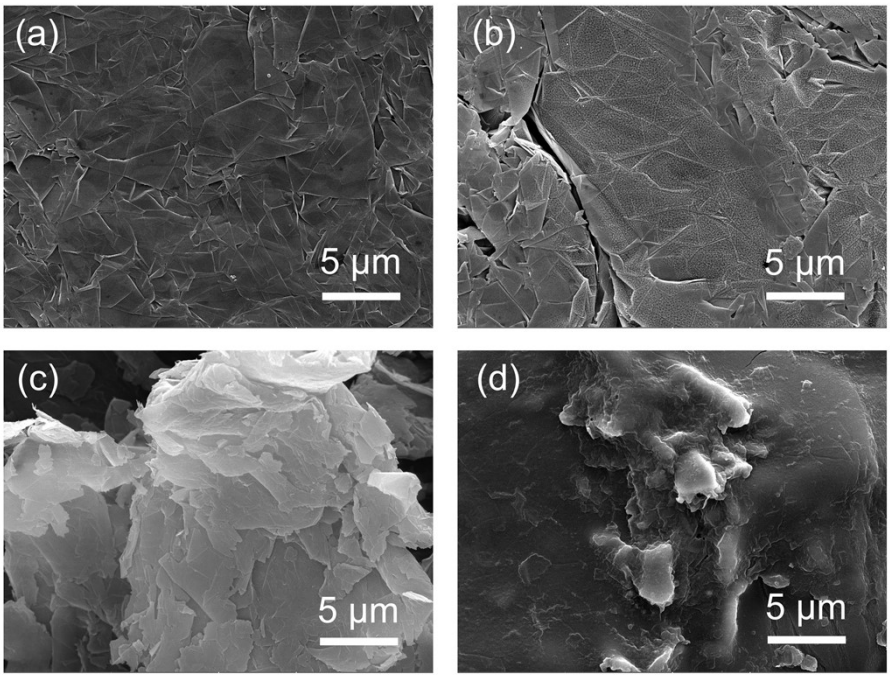


Fig. S4. SEM of (a) Graphite, (b) Graphite@Au, (c) Graphene, and (d) Gelatin-0.04/0.06 M $FeCN^{4-/3-}$-6 wt.% Gr.

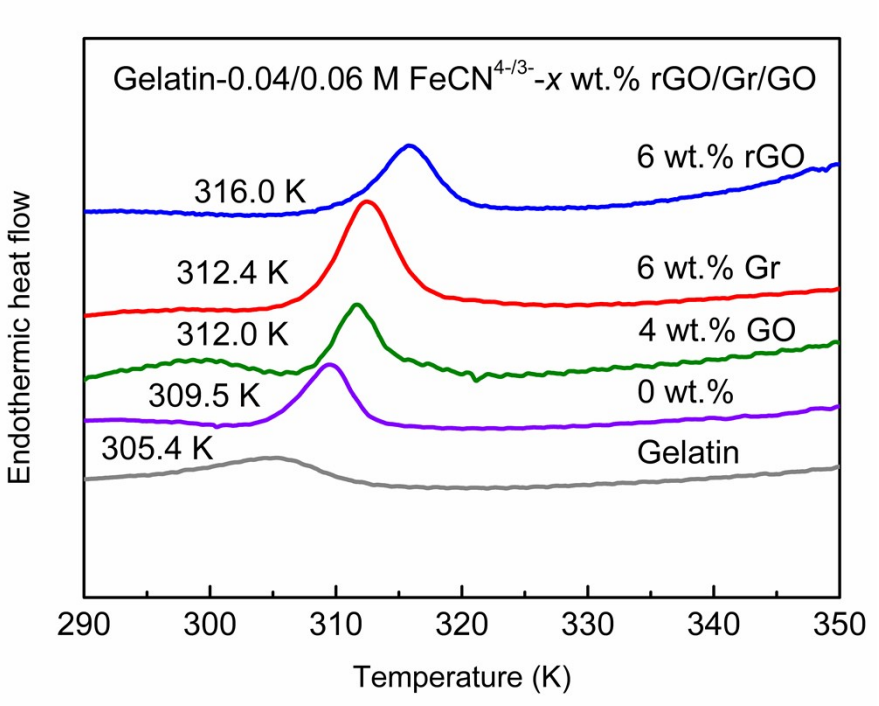


Fig. S5. DSC curves of Gelatin and Gelatin-0.04/0.06 M $FeCN^{4-/3-}$-*x* wt.% rGO/Gr/GO (*x* = 0, 4, 6).

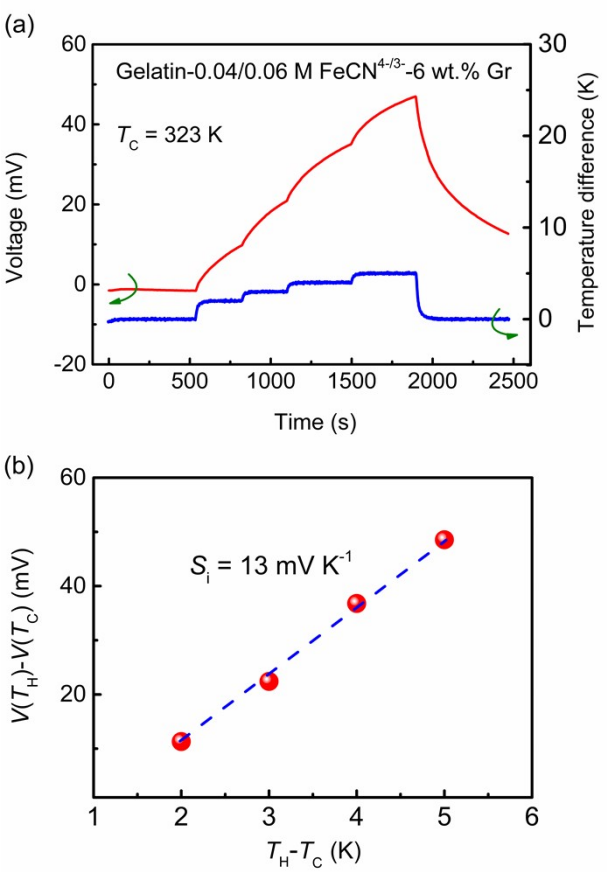


Fig. S6. (a) Voltage and temperature with dependence of time; (b) $V(T_H)$-$V(T_C)$ with dependence of $T_H$-$T_C$ for gels Gelatin-0.04/0.06 M $FeCN^{4-/3-}$-6 wt.% Gr.

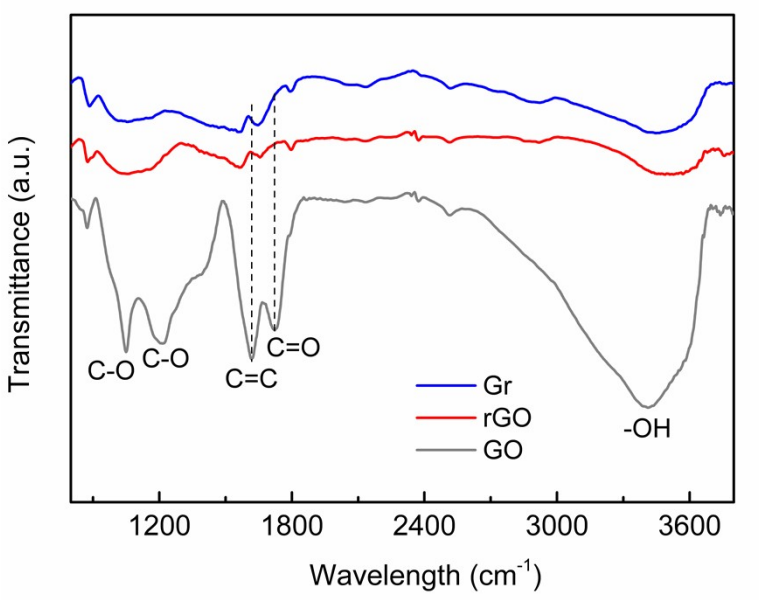


Fig. S7. Fourier transform infrared spectroscopy (FTIR) of Gr, rGO and GO.

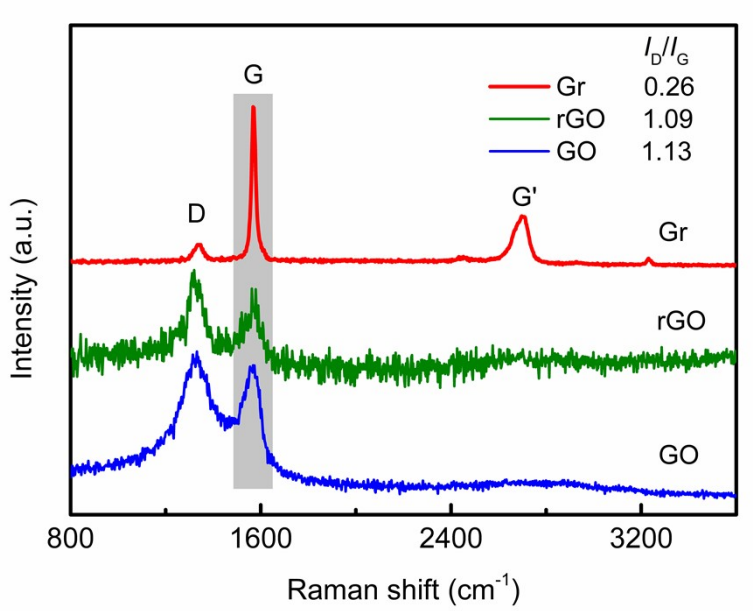


Fig. S8. Raman spectroscopy of Gr, rGO and GO. The wavelength laser was 532 nm.

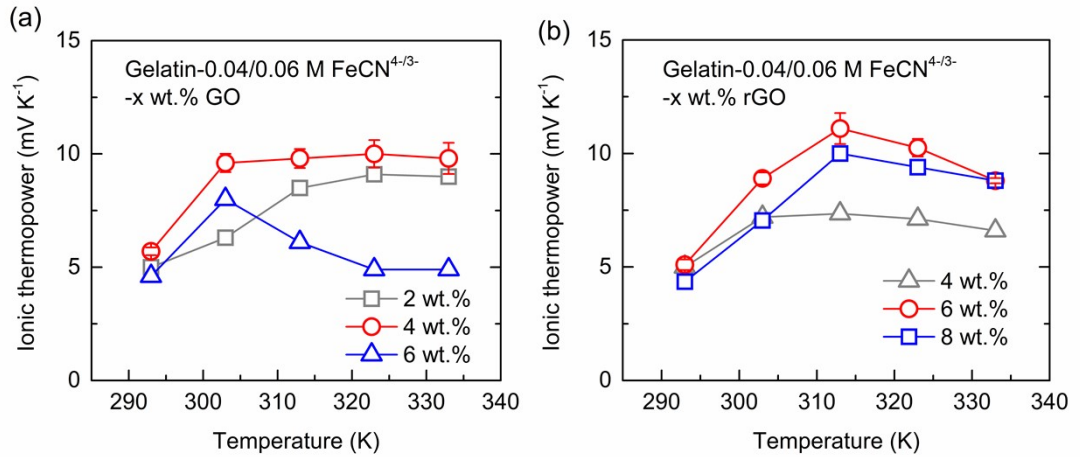


Fig. S9. Ionic thermopower with dependence of temperature. (a) Gelatin-0.04/0.06 M $FeCN^{4-/3-}$-*x* wt.% GO (*x* = 2, 4, 6), (b) Gelatin-0.04/0.06 M $FeCN^{4-/3-}$-*x* wt.% rGO (*x* = 4, 6, 8).

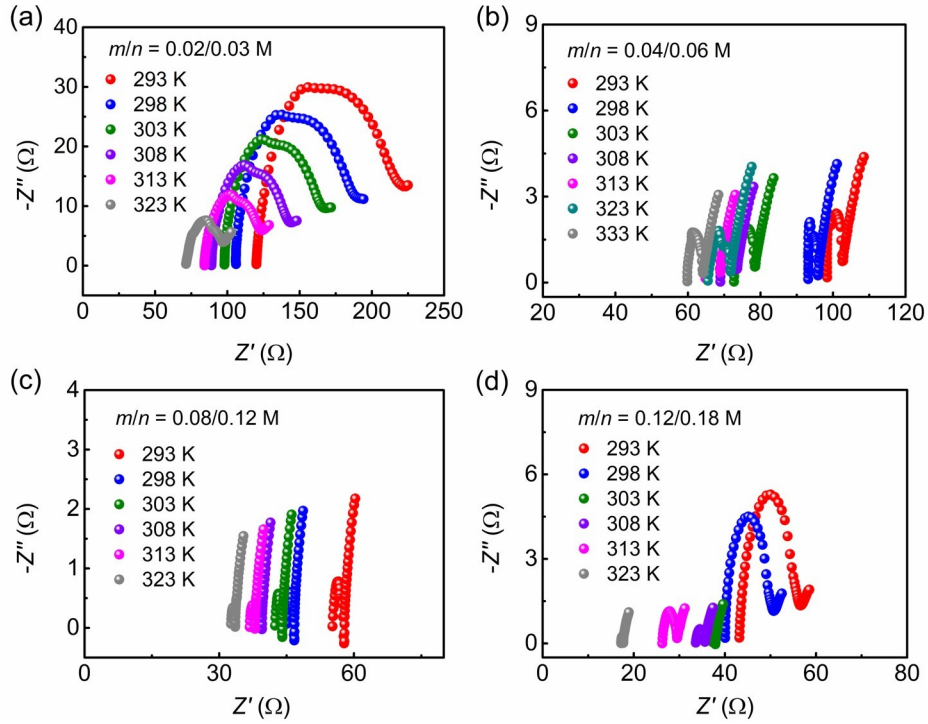


Fig. S10. Electrochemical impedance spectroscopy (EIS) of gels Gelatin-*m*/*n* $FeCN^{4-/3-}$ for (a) *m*/*n* = 0.02/0.03 M, (b) *m*/*n* = 0.04/0.06 M, (c) *m*/*n* = 0.08/0.12 M, and (d) *m*/*n* = 0.12/0.18 M, respectively.

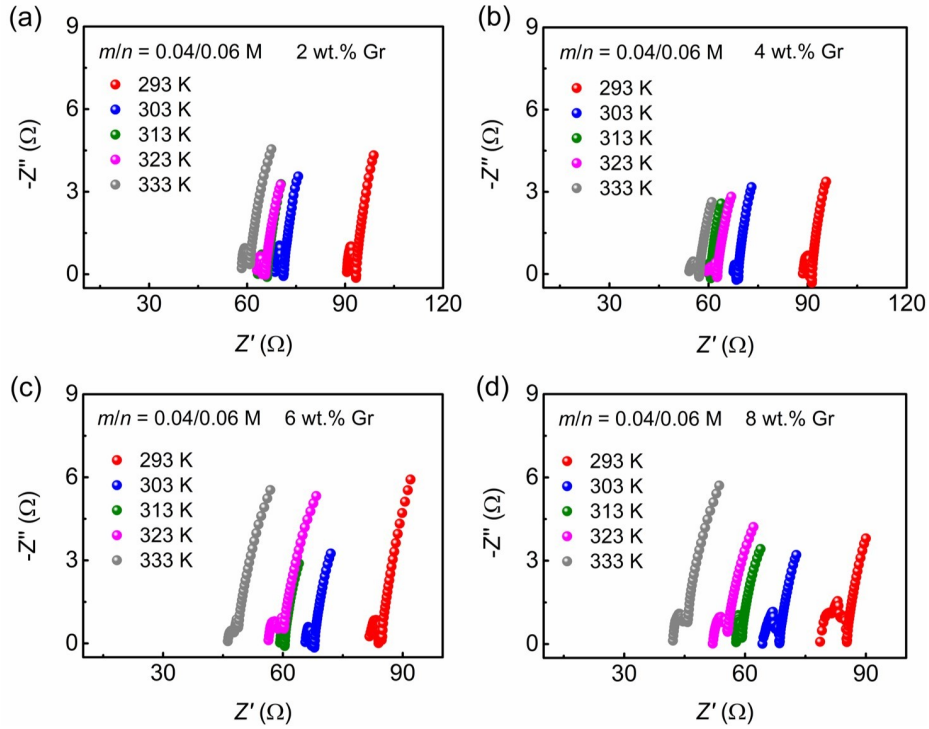


Fig. S11. Electrochemical impedance spectroscopy (EIS) of gels Gelatin-0.04/0.06 M $FeCN^{4-/3-}$-*x* wt.% Gr for (a) *x* = 2, (b) *x* = 4, (c) *x* = 6, (d) *x* = 8, respectively.

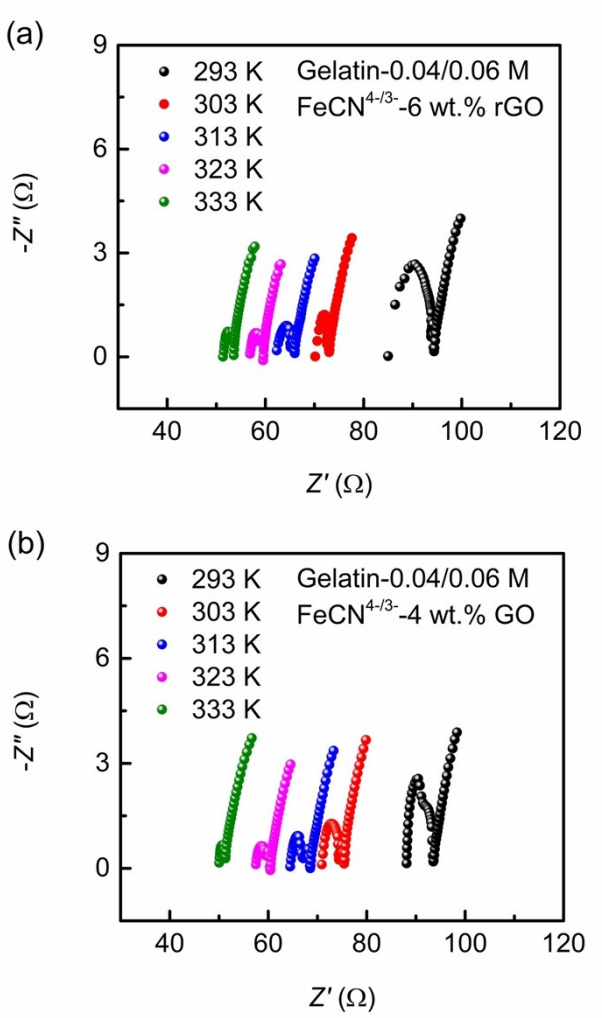


Fig. S12. Electrochemical impedance spectroscopy (EIS) of gels (a) Gelatin-0.04/0.06 M $FeCN^{4-/3-}$-6 wt.% rGO and (b) Gelatin-0.04/0.06 M $FeCN^{4-/3-}$-4 wt.% GO.

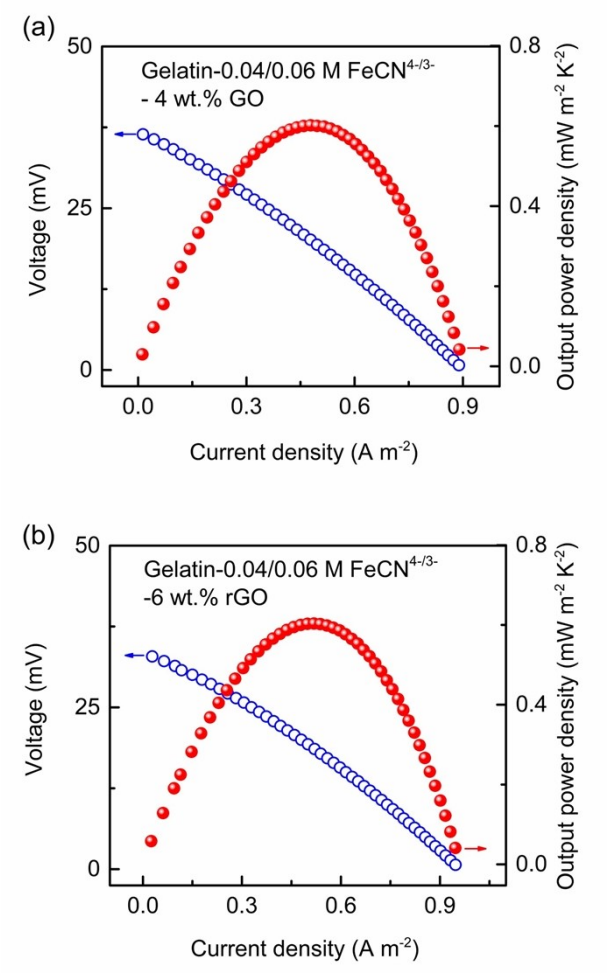


Fig. S13. Voltage and output power density with dependence of current density for gels (a) Gelatin-0.04/0.06 M $FeCN^{4-/3-}$-4 wt.% GO and (b) Gelatin-0.04/0.06 M $FeCN^{4-/3-}$-6 wt.% rGO.

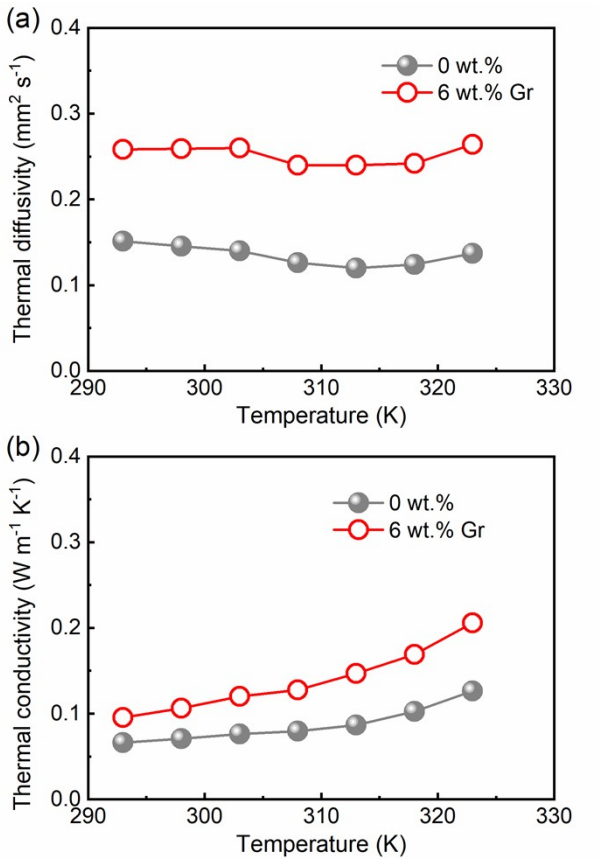


Fig. S14. (a) Thermal diffusivity and (b) Thermal conductivity with dependence of temperature for gels Gelatin-0.04/0.06 M $FeCN^{4-/3-}$-*x* wt.% Gr (*x* = 0, 6).

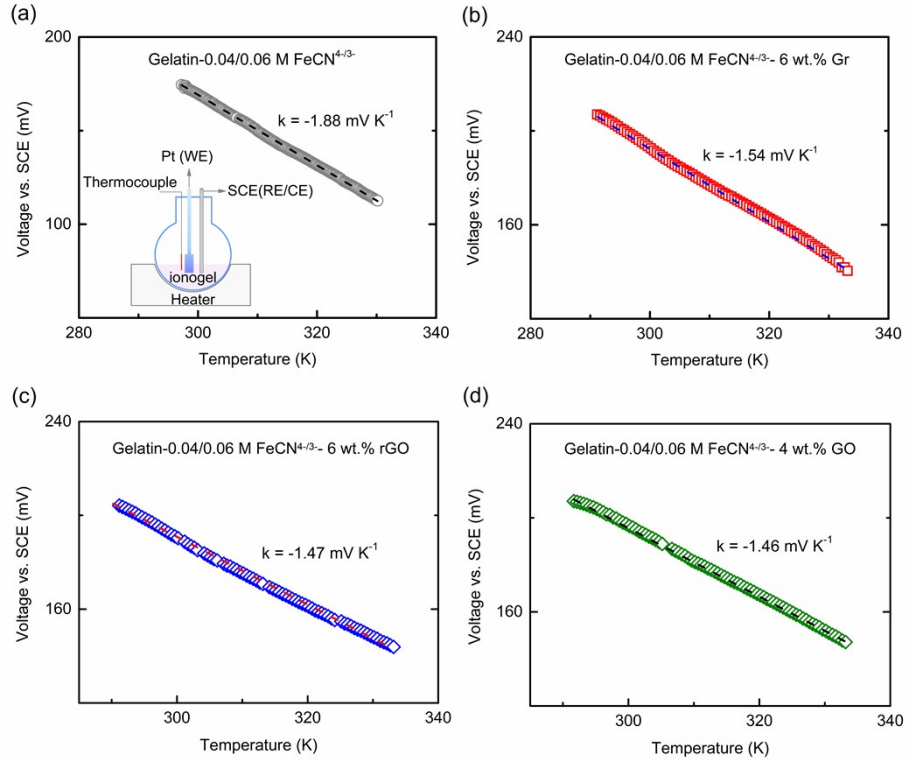


Fig. S15. Voltage vs. SCE with dependence of temperature in an isothermal system for gels Gelatin-0.04/0.06 M $FeCN^{4-/3-}$-*x* wt.% Gr/rGO/GO with (a) 0 wt.%, (b) 6 wt.% Gr, (c) 6 wt.% rGO and (d) 4 wt.% GO. The picture of isothermal system was shown in the insert of (a). Platinum was served as work electrode (WE), while SCE was used as reference electrode (RE) and counter electrode (CE). For an isothermal system in electrochemistry community, temperature coefficient referred to a temperature dependence of the standard electrode potential ($E_0$), which was defined as $\alpha_R = dE_0/dT$. $\alpha_R$ = -1.88, -1.54, -1.47 and -1.46 mV $K^{-1}$ are observed for 0 wt.%, 6 wt.% Gr, 6 wt.% rGO and 4 wt.% GO, respectively, whereas that of SCE is -0.47 mV $K^{-1}$.[S11] Based on the thermogalvanic effect, ionic thermopower was $S_{tg} = -\alpha_R$.[S2] Therefore, ionic thermopower $S_{tg}$ ($FeCN^{4-/3-}$) is 2.35, 2.01, 1.94 and 1.93 mV $K^{-1}$ for 0 wt.%, 6 wt.% Gr, 6 wt.% rGO and 4 wt.% GO, respectively.

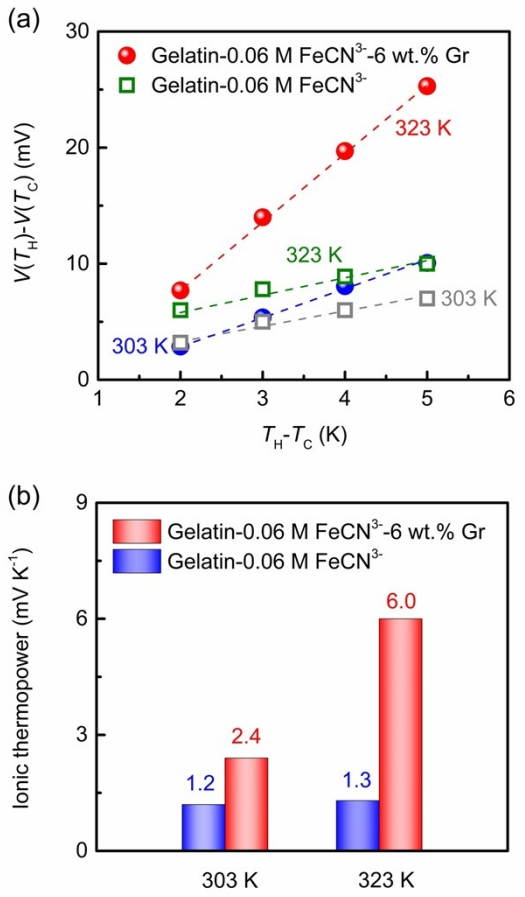


Fig. S16. (a) $V(T_H)$-$V(T_C)$ with dependence of $T_H$-$T_C$, and (b) ionic thermopower for gels Gelatin-0.06 M $FeCN^{3-}$-$x$ wt.% Gr ($x$ = 0, 6) at 303 K and 323 K.

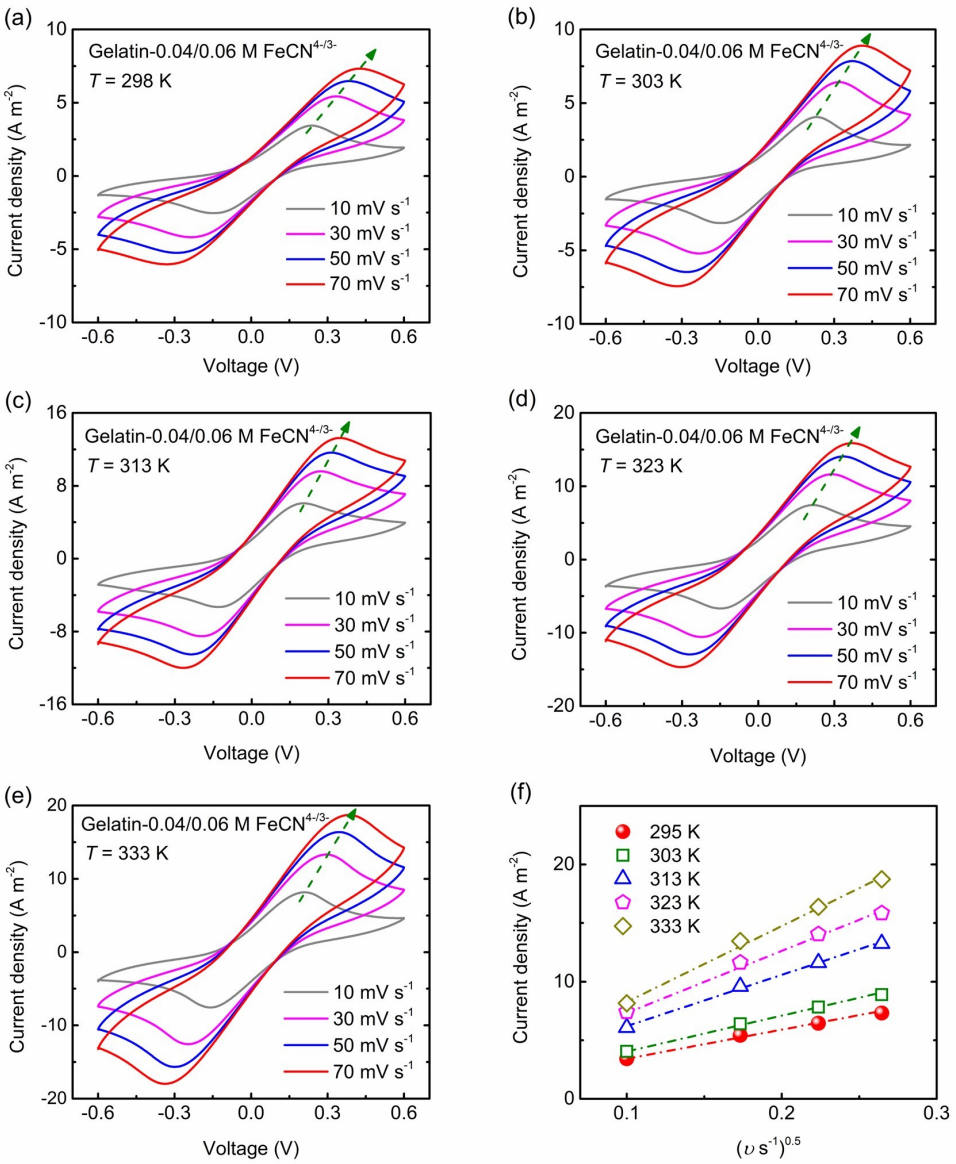


Fig. S17. Cyclic voltammetry (CV) of gels Gelatin-0.04/0.06 M $FeCN^{4-/3-}$ at different temperatures of (a) 298 K, (b) 303 K, (c) 313 K, (d) 323 K and (e) 333 K. (f) Current density with dependence of $(\upsilon\ s^{-1})^{0.5}$. The scan rates are $\upsilon$ = 10, 30, 50, 70 mV $s^{-1}$, respectively.

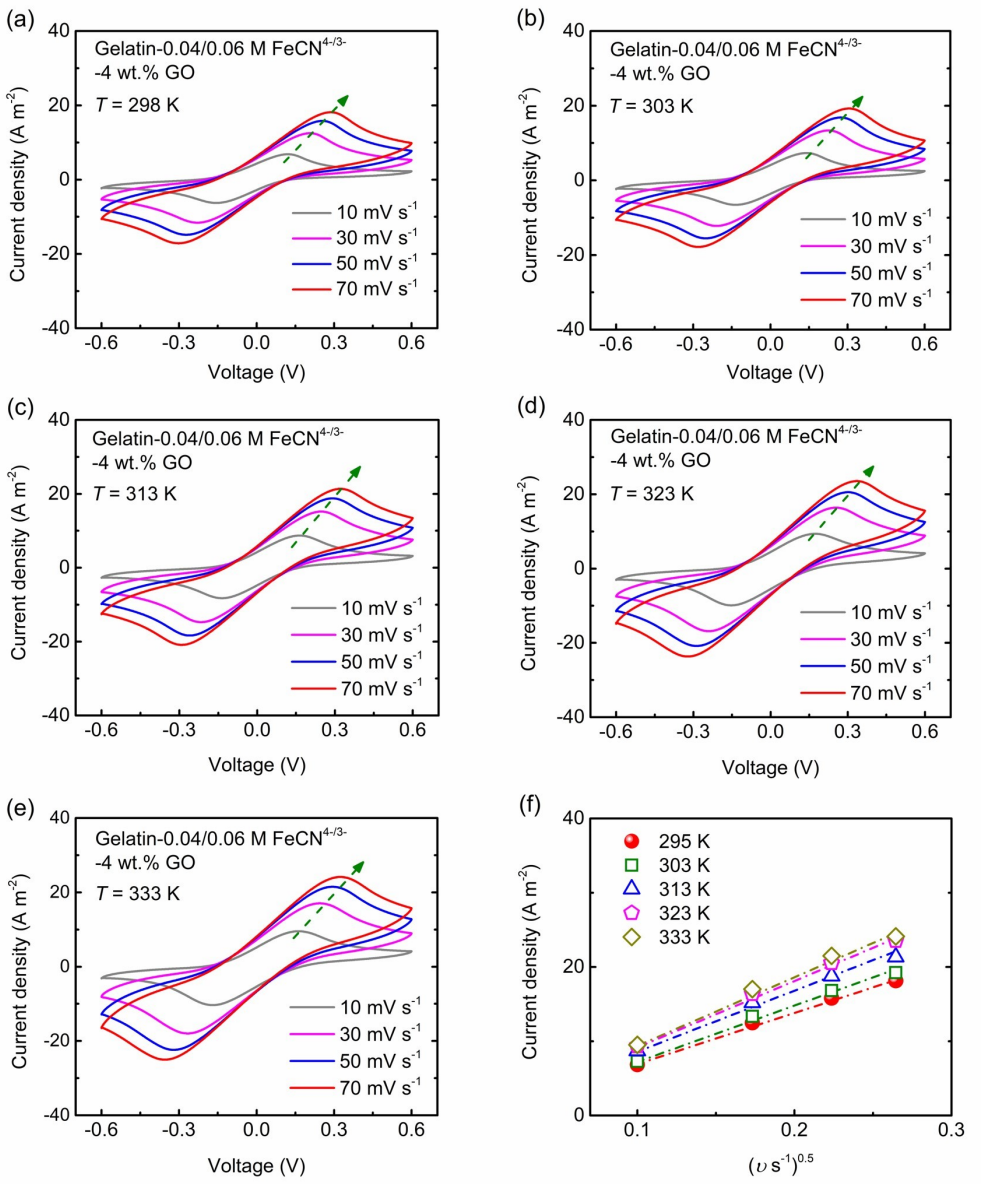


Fig. S18. Cyclic voltammetry (CV) of gels Gelatin-0.04/0.06 M $FeCN^{4-/3-}$-4 wt.% GO at different temperatures of (a) 298 K, (b) 303 K, (c) 313 K, (d) 323 K and (e) 333 K. (f) Current density with dependence of $(\upsilon\ s^{-1})^{0.5}$.

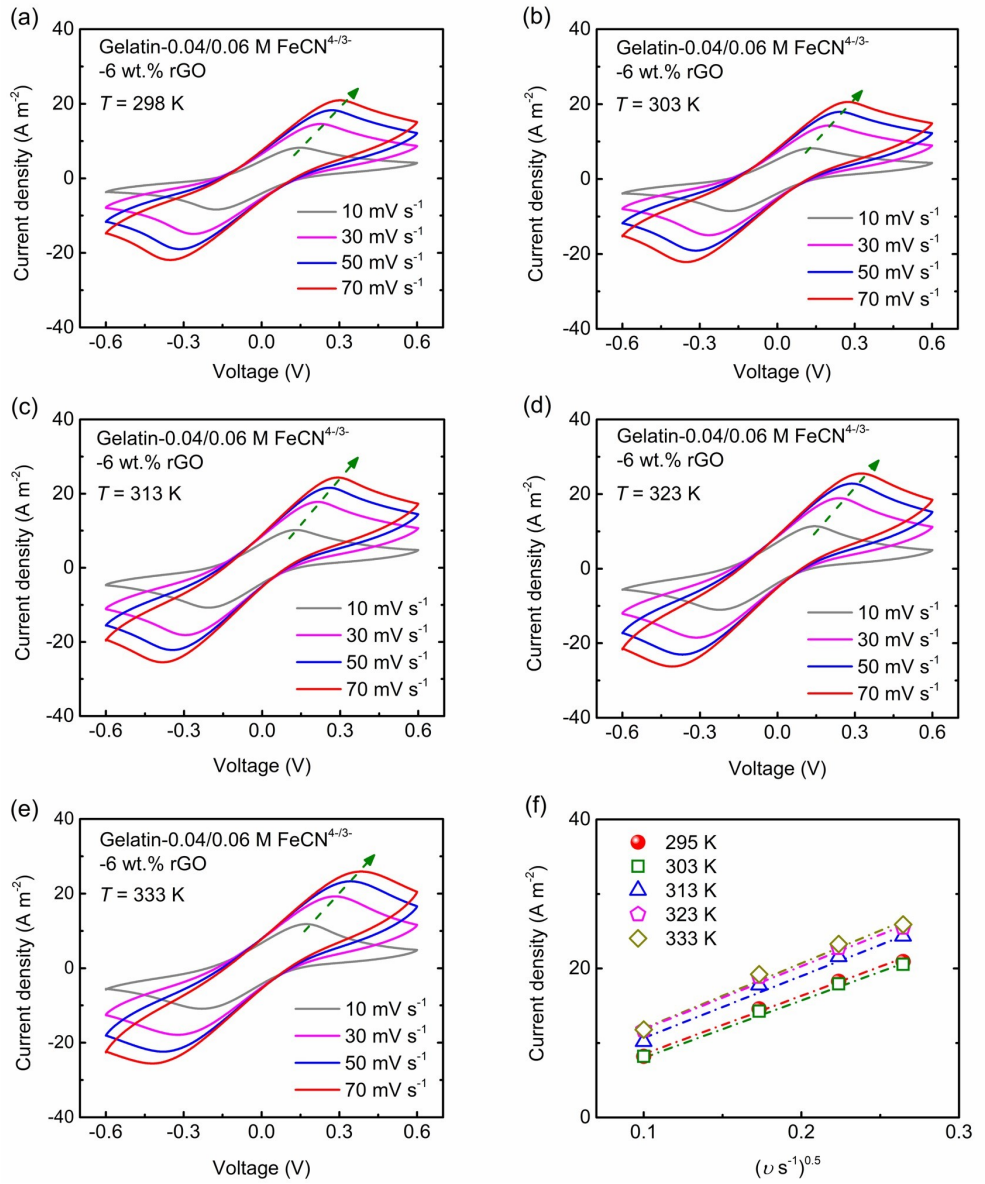


Fig. S19. Cyclic voltammetry (CV) of gels Gelatin-0.04/0.06 M $FeCN^{4-/3-}$-6 wt.% rGO at different temperatures of (a) 298 K, (b) 303 K, (c) 313 K, (d) 323 K and (e) 333 K. (f) Current density with dependence of $(\upsilon\ s^{-1})^{0.5}$.

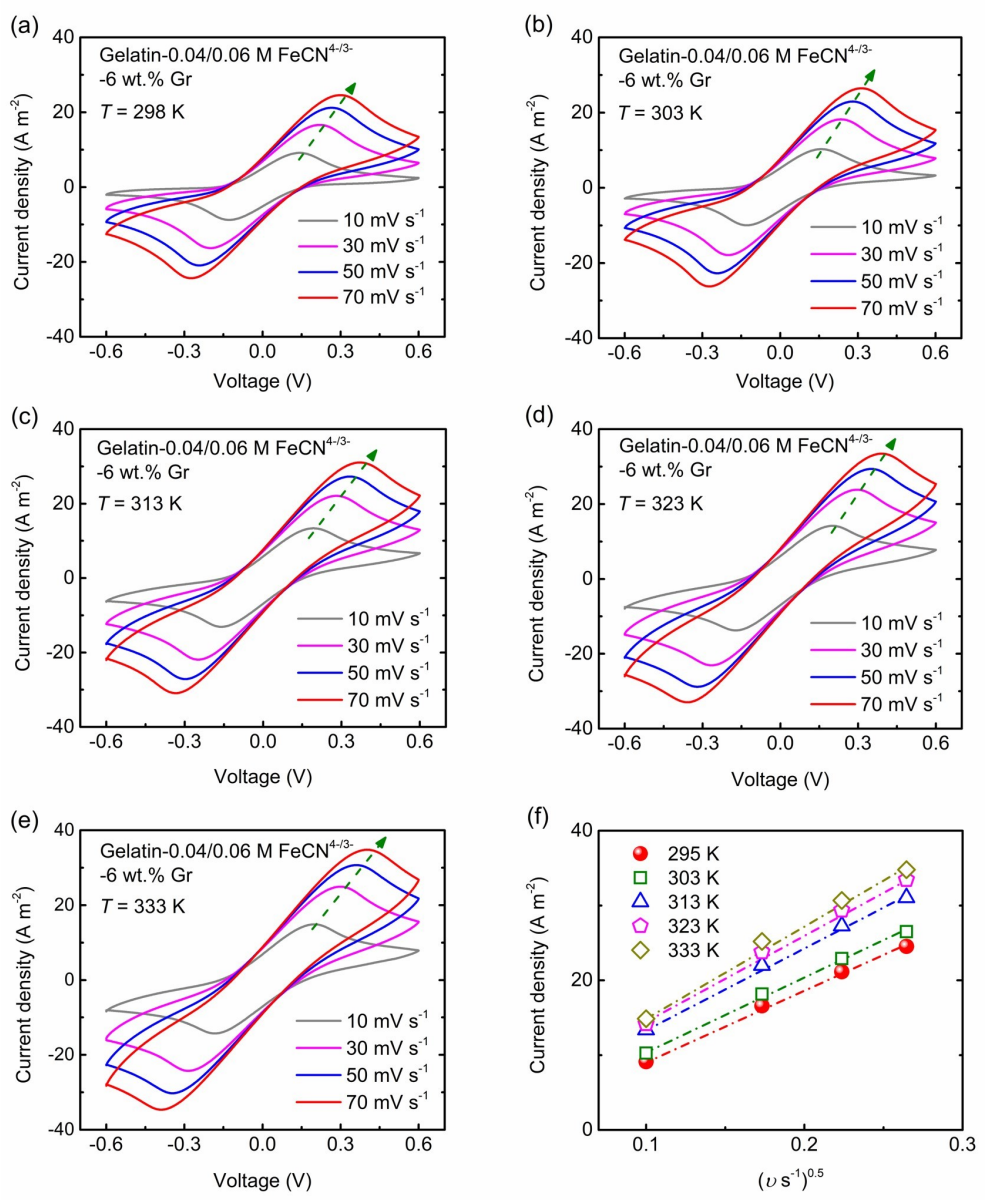


Fig. S20. Cyclic voltammetry (CV) of gels Gelatin-0.04/0.06 M $FeCN^{4-/3-}$-6 wt.% Gr at different temperatures of (a) 298 K, (b) 303 K, (c) 313 K, (d) 323 K and (e) 333 K. (f) Current density with dependence of $(\upsilon\ s^{-1})^{0.5}$.

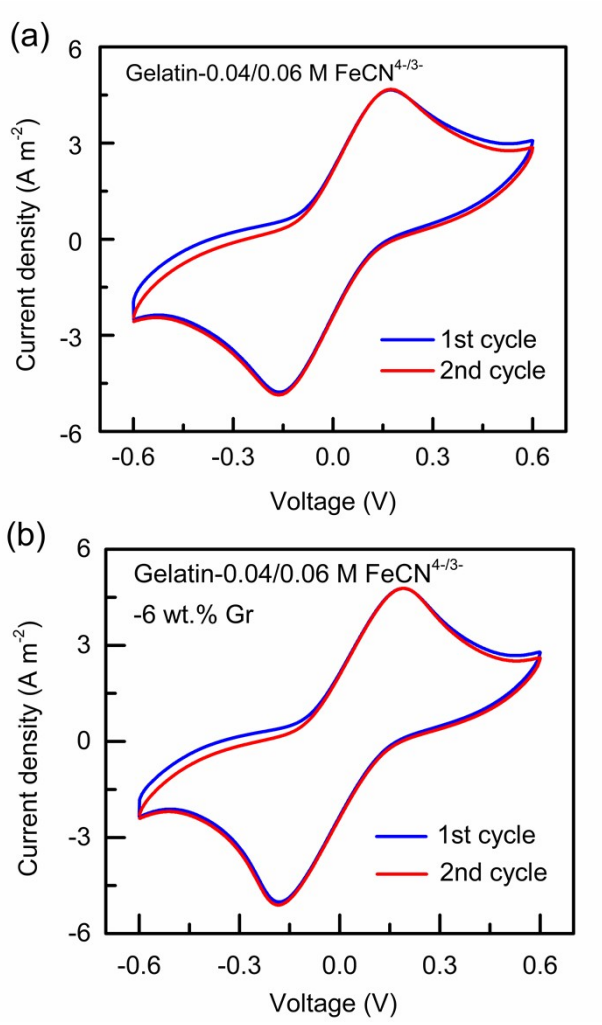


Fig. S21. Cyclic voltammetry (CV) of Gelatin-0.04/0.06 M $FeCN^{4-/3-}$ -*x* wt.% Gr (a) *x* = 0, (b) *x* = 6. The scan rate was 10 mV $s^{-1}$. Graphite@Au was employed as electrodes.

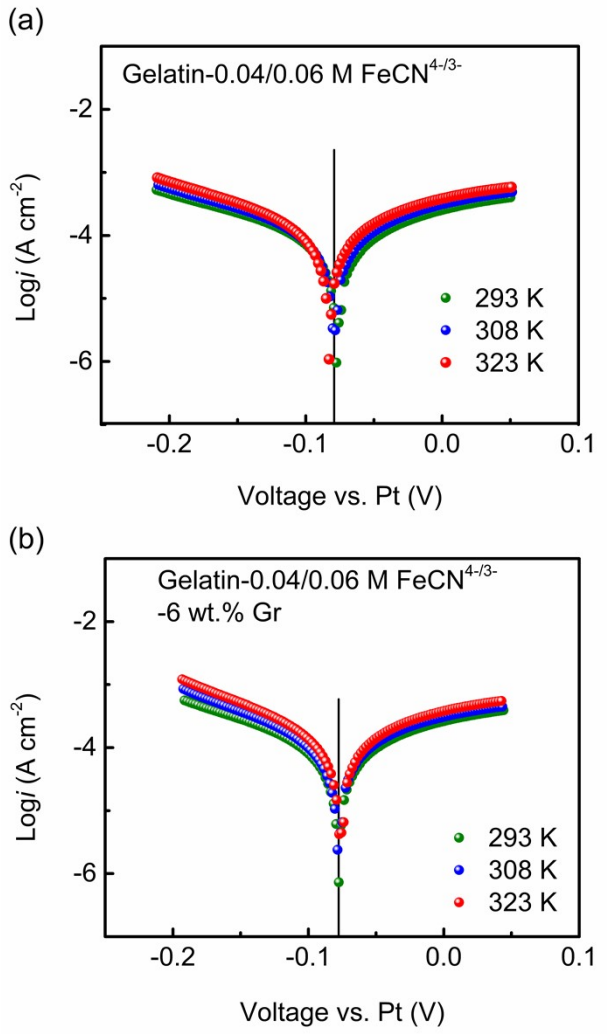


Fig. S22. Tafel curves of Gelatin-0.04/0.06 M $FeCN^{4-/3-}$-*x* wt.% Gr for (a) *x* = 0 and (b) *x* = 6. Pt was employed as electrodes.

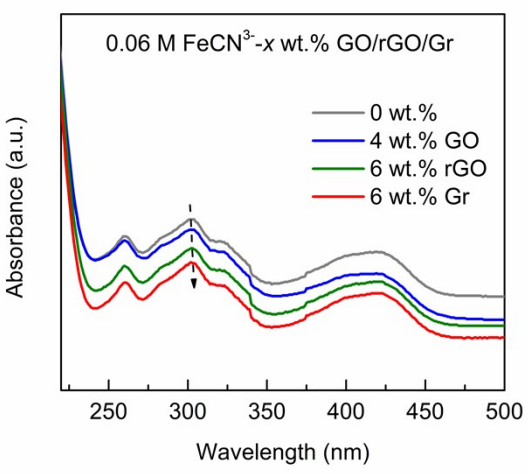


Fig. S23. Ultraviolet and visible spectrophotometry (UV-Vis) of aqueous 0.06 M $FeCN^{3-}$-*x* wt.% GO/rGO/Gr (*x* = 0, 4, 6).

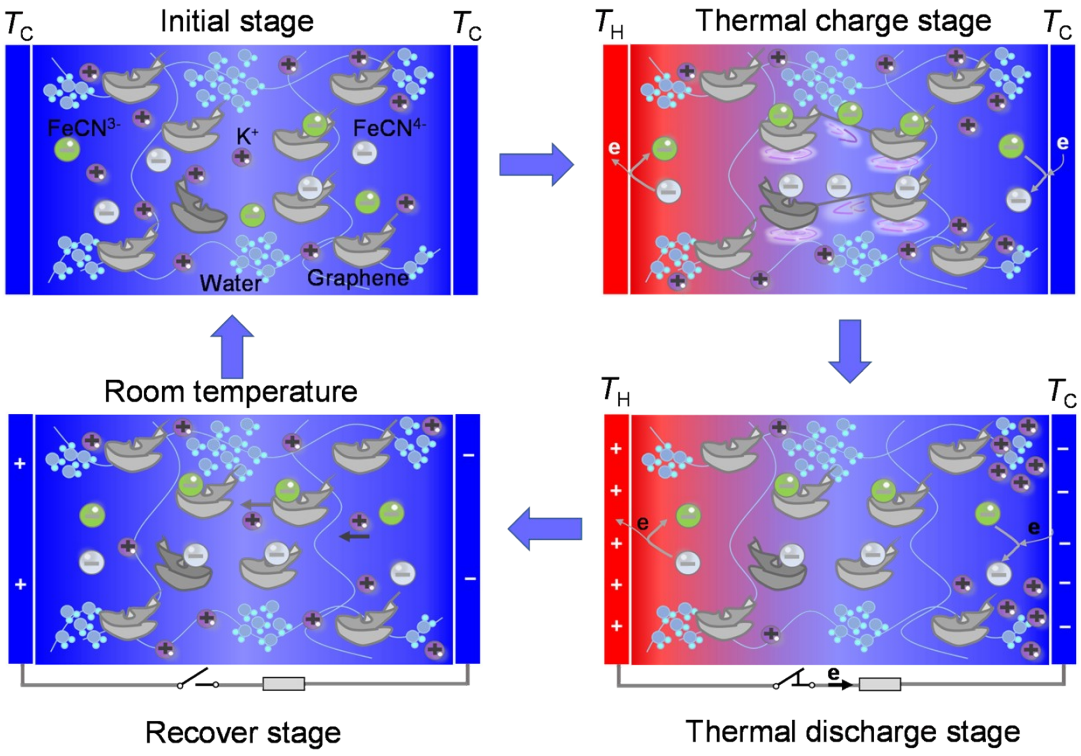


Fig. S24. Schematic image of redox reaction and ions migration in gels Gelatin-*m*/*n* $FeCN^{4-/3-}$ -*x* wt.% Gr, including initial stage, thermal charge stage, thermal discharge stage and recover stage.

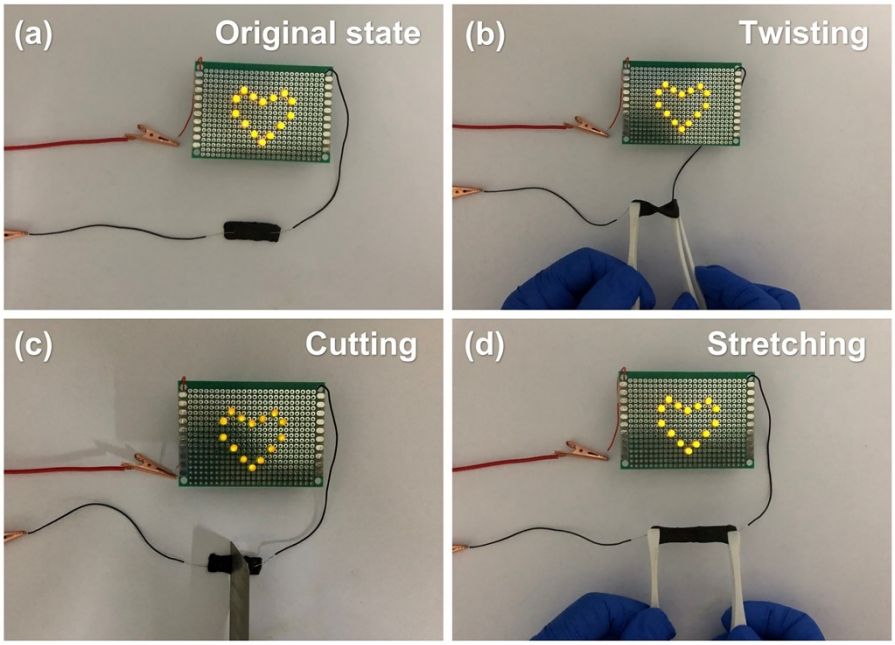


Fig. S25. Conductivity of gels Gelatin-0.04/0.06 M $FeCN^{4-/3-}$-6 wt.% Gr under different mechanical treatments. (a) Original state, (b) Twisting, (c) Cutting, (d) Stretching.

Table S1. Comparison of ionic thermopower and output power density $P_{max}/(\Delta T)^2$ for this work and reported values.

| Gels | Ionic thermopower ($mV\ K^{-1}$) | $P_{max}/(\Delta T)^2$ ($mW\ m^{-2}\ K^{-2}$) | Reference |
|---|---|---|---|
| Gelatin-$FeCN^{4-/3-}$-graphene | 13 | 1.03 | This work |
| P(AM-co-AMPS)- $FeCN^{4-/3-}$ | 1.6 | 0.61 | S12 |
| Gelatin-$FeCN^{4-/3-}$-KCl | 12.7 | 0.66 | S2 |
| MC-$I^-/I_3^-$-KCl | 9.6 | 0.36 | S13 |
| PAAm-$FeCN^{4-/3-}$ | 1.37 | 0.31 | S14 |
| PVA-SO2- 4/3 | 1.63 | 0.0003 | S15 |
| Bacterial cellulose-$FeCN^{4-/3-}$ | 4.5 | 0.024 | S16 |
| PVA/ $FeCN^{4-/3-}$ | 1.5 | 0.22 | S17 |
| PVA/$FeCN^{4-/3-}$ | 1.21 | 0.024 | S18 |

Table S2. Comparison of normalized energy density for this work and reported values.

| Gels | Energy density ($J\ m^{-2}\ K^{-2}$) | Time (h) | $\Delta T$ (K) | Reference |
|---|---|---|---|---|
| Gelatin-$FeCN^{4-/3-}$-graphene | 0.19 | 1 | 4 | This work |
| CaBC-NaCl | 0.10 | 1 | 5.5 | S19 |
| PPP-$SiO_2$ | 0.006 | 4.2 | 1.8 | S20 |
| PVDF-HFP/NaTFSI/PC (PhNP) | 0.004 | 0.1 | 1.5 | S21 |
| Gelatin-[EMIM] DCA | 0.0001 | 2 | 10 | S22 |
| PEO-NaOH | 0.0003 | - | 4.5 | S23 |
| PSS/H/GO | 0.022 | - | 9.5 | S24 |
| $SiO_2$-IL | 0.016 | - | 4 | S25 |
| PVDF-HFP | 0.009 | - | 0.6 | S26 |

Table S3. Comparison of output power density $P_{max}/(\Delta T)^2$ of gels devices for this work and reported values.

| Gels | $P_{max}/(\Delta T)^2$ of device (mW m$^{-2}$ K$^{-2}$) | Cell number | Reference |
|---|---|---|---|
| Gelatin-$FeCN^{4-/3-}$-graphene | 1.2 | 4 | This work |
| PVA/$FeCN^{4-/3-}$ | 0.024 | 2 | S18 |
| bacterial cellulose-$FeCN^{4-/3-}$ | 0.024 | 6 | S16 |
| PNIPAM-$I^-/I_3^-$ | 0.072 | 100 | S27 |
| Gelatin-$FeCN^{4-/3-}$-KCl | 0.08 | 25 | S2 |
| Gelatin-$FeCN^{4-/3-}$-KCl | 0.13 | 24 | S28 |
| Gelatin-$FeCN^{4-/3-}$-KCl | 0.43 | 16 | S29 |
| PVA/$FeCN^{4-/3-}$ | 0.512 | 27 | S17 |

**References**


[S1] S. W. Boettcher, S. Z. Oener, M. C. Lonergan, Y. Surendranath, S. Ardo, C. Brozek and P. A. Kempler, Potentially confusing: potentials in electrochemistry, *ACS Energy Lett*., 2021, **6**, 261-266.

[S2] C.-G. Han, X. Qian, Q. K. Li, B. Deng, Y. B. Zhu, Z. J. Han, W. Q. Zhang, W. C. Wang, S.-P. Feng, G. Chen and W. S. Liu. Giant thermopower of ionic gelatin near room temperature. *Science*, 2020, **368**, 1091-1098.

[S3] D. Voiry, J. Yang, J. Kupferberg, R. Fullon, C. Lee, H. Y. Jeong, H. S. Shin and M. Chhowalla, High-quality graphene via microwave reduction of solution-exfoliated graphene oxide, *Science*, 2016, **353**, 1413-1416.

[S4] J. Song, X. Wang and C.-T. Chang, Preparation and characterization of graphene oxide, *J. Nanomater.*, 2014, **2014**, 276143.

[S5] H.-Y. Hu, N. Xie, C. Wang, L.-Y. Wang, R. M. Privette, H.-F. Li, M. Pan, F. Wu, X.-L. Yan, B.-B. Jiang, M. H. Wu, K. Vinodgopal and G.-P. Dai, Enhanced performance of E-bike motive power lead-acid batteries with graphene as an additive to the active mass, *ACS Omega*, 2018, **3**, 7096-7105.

[S6] J.-B. Wu, M.-L. Lin, X. Cong, H.-N. Liu and P.-H. Tan, Raman spectroscopy of graphene-based materials and its applications in related devices, *Chem. Soc. Rev*., 2018, **47**, 1822-1873.

[S7] V. B. Mohan, M. Nieuwoudt, K. Jayaraman and D. Bhattacharyya, Quantification and analysis of Raman spectra of graphene materials, *Graphene Technol*., 2017, **2**, 47-62.

[S8] L. M. Malard, M. A. Pimenta, G. Dresselhaus and M. S. Dresselhaus, Raman spectroscopy in graphene, *Phys. Rep*., 2009, **473**, 51-87.

[S9] J. Daintith, A Dictionary of Chemistry (6 ed.), Oxford University Press, 2008.

[S10] A. L. Bard and L. Faulkner. Electrochemical methods: Fundamentals and applications, 2nd edition. John Wiley & Sons, 2001.

[S11] A. J. deBethune, T. S. Licht and N. Swendeman. The temperature coefficients of electrode potentials. *J. Electrochem. Soc.*, 1959, **106**, 616-625.

[S12] Z. Y. Lei, W. Gao and P. Y. Wu. Double-network thermocells with extraordinary toughness and boosted power density for continuous heat harvesting. *Joule*, 2021, **5**, 2211-2222.

[S13] Y. Han, J. Zhang, R. Hu and D. Y. Xu. High-thermopower polarized electrolytes enabled by methylcellulose for low-grade heat harvesting. *Sci. Adv.*, 2022, **8**, eabl5318.

[S14] C. Xu, Y. Sun, J. J. Zhang, W. Xu and H. Tian. Adaptable and wearable thermocell based on stretchable hydrogel for body heat harvesting. *Adv. Energy Mater.*, 2022, **12**, 2201542.

[S15] C. H. Tian, C. H. Bai, T. Wang, Z. F. Yan, Z. Y. Zhang, K. Zhuo and H. L. Zhang. Thermogalvanic hydrogel electrolyte for harvesting biothermal energy enabled by a novel redox couple of SO2- 4/3 ions. *Nano Energy*, 2023, **106**, 108077.

[S16] Y. D. Zong, H. B. Li, X. Li, J. Lou, Q. J. Ding, Z. Q. Liu, Y. F. Jiang and W. J. Han. Bacterial cellulose-based hydrogel thermocells for low-grade heat harvesting. *Chem. Eng. J.*, 2022, **433**, 134550.

[S17] W. Gao, Z. Y. Lei, W. W. Chen and Y. P. Chen. Hierarchically anisotropic networks to decouple mechanical and ionic properties for high-performance auasi-solid thermocells. *ACS Nano*, 2022, **16**, 8347-8357.

[S18] P. H. Yang, K. Liu, Q. Chen, X. B. Mo, Y. S. Zhou, S. Li, G. Feng and J. Zhou. Wearable thermocells based on gel electrolytes for the utilization of body heat. *Angew. Chem. Int. Ed.*, 2016,

**55**, 12050-12053.

[S19] Z. T. Wu, B. X. Wang, J. Li, R. L. Wu, M. T. Jin, H. W. Zhao, S. Y. Chen and H. P. Wang. Advanced bacterial cellulose ionic conductors with gigantic thermopower for low-grade heat harvesting. *Nano Lett.*, 2022, **22**, 8152-8160.

[S20] Y. T. Malik, Z. A. Akbar, J. Y. Seo, S. Cho, S.-Y. Jang and J.-W. Jeon. Self-healable organic–inorganic hybrid thermoelectric materials with excellent ionic thermoelectric properties. *Adv. Energy Mater.*, 2022, **12**, 2103070.

[S21] C. Chi, M. An, X. Qi, Y. Li, R. H. Zhang, G. Z. Liu, C. J. Lin, H. Huang, H. Dang, B. Demir, Y. Wang, W. G. Ma, B. L. Huang and X. Zhang. Selectively tuning ionic thermopower in all-solid-state flexible polymer composites for thermal sensing. *Nat. commun.*, 2022, **13**, 221.

[S22] J. L. Ke, X. Zhao, J. Yang, K. Ke, Y. Wang, M. B. Yang and W. Yang. Enhanced ion-selective diffusion achieved by supramolecular interaction for high thermovoltage and thermal stability. *Energy Environ. Mater.*, 2022, **0**, e12562.

[S23] D. Zhao, H. Wang, Z. U. Khan, J. C. Chen, R. Gabrielsson, M. P. Jonsson, M. Berggren and X. Crispin. Ionic thermoelectric supercapacitors. *Energy Environ. Sci.*, 2016, **9**, 1450-1457.

[S24] M. Jeong, J. Noh, M. Z. Islam, K. Kim, A. Sohn, W. Kim and C. Yu. Embedding aligned graphene oxides in polyelectrolytes to facilitate thermo-diffusion of protons for high ionic thermoelectric figure-of-merit. *Adv. Funct. Mater.*, 2021, **31**, 2011016.

[S25] X. He, H. L. Cheng, S. Z. Yue and J. Y. Ouyang. Quasi-solid state nanoparticle/(ionic liquid) gels with significantly high ionic thermoelectric properties. *J. Mater. Chem. A*, 2020, **8**, 10813-10821.

[S26] H. L. Cheng, X. He, Z. Fan and J. Y. Ouyang. Flexible quasi-solid state ionogels with remarkable seebeck coefficient and high thermoelectric properties. *Adv. Energy Mater.*, 2019, **9**, 1901085.

[S27] J. J. Duan, B. Y. Yu, K. Liu, J. Li, P. H. Yang, W. K. Xie, G. B. Xue, R. Liu, H. Wang and J. Zhou. P-N conversion in thermogalvanic cells induced by thermo-sensitive nanogels for body heat harvesting. *Nano Energy*, 2019, **57**, 473-479.

[S28] Y. C. Li, Q. K. Li, X. B. Zhang, B. Deng, C. G. Han and W. S. Liu. 3D hierarchical electrodes boosting ultrahigh power output for Gelatin-KCl-$FeCN^{4-/3-}$ ionic thermoelectric cells. *Adv. Energy Mater.*, 2022, **12**, 2103666.

[S29] Y. C. Li, Q. K. Li, X. B. Zhang, J. J. Zhang, S. H. Wang, L. Q. Lai, K. Zhu and W. S. Liu. Realizing record-high output power in flexible gelatin/GTA-KCl-$FeCN^{4-/3-}$ ionic thermoelectric cells enabled by extending the working temperature range. *Energy Environ. Sci.*, 2022, **15**, 5379-5390.